International Journal of Nanomedicine

Dovepress
Taylor & Francis Group

Open Access Full Text Article

ORIGINAL RESEARCH

# Pd Icosahedral Nanoparticles Promote Skin Wound Healing by Enhancing SP1-HBEGF Axis-Mediated Keratinocytes Proliferation

Fanping He[1–3,*], Mengfan Li[4,*], Han Zhao[1,3], He Zhao[1,3], Xin Meng[1,3], Yiya Zhang[1,3,5], Yan Tang[1,3,5], Hongwen Huang[4,6], Ji Li[1,3,5], Hongfu Xie[1,3], Ben Wang[1,3,5]

[1]Department of Dermatology, Xiangya Hospital, Central South University, Changsha, People's Republic of China; [2]Department of Plastic and Reconstructive Surgery, Beijing Tongren Hospital, Capital Medical University, Beijing, People's Republic of China; [3]Hunan Key Laboratory of Aging Biology, Xiangya Hospital, Central South University, Changsha, People's Republic of China; [4]College of Materials Science and Engineering, Hunan University, Changsha, Hunan, 410082, People's Republic of China; [5]National Clinical Research Center for Geriatric Disorders, Xiangya Hospital, Central South University, Changsha, Hunan, 410008, People's Republic of China; [6]Shenzhen Research Institute of Hunan University, Shenzhen, Guangdong, 518055, People's Republic of China

*These authors contributed equally to this work

Correspondence: Ben Wang; Hongfu Xie, Email wangben@csu.edu.cn; xiehongfu@csu.edu.cn

**Introduction:** Impaired wound healing leads to compromised cutaneous barrier and dysfunction, which still remains a challenging problem. However, safe and efficient materials and treatments for promoting wound healing are still lacking. Metal nanoparticles especially palladium nanoparticles (Pd NPs) have attracted tremendous interests in medical application in recent years, due to its unique physicochemical properties and biological inertness. Thereinto, Pd icosahedra nanoparticles (Pd Icos NPs) and Pd octahedra nanoparticles (Pd Oct NPs) have superior catalytic activity compared to other shapes but the application in skin wound healing have not been studied and reported.

**Methods:** Pd Oct NPs and Pd Icos NPs were synthesized by seed-mediated growth method and one-step synthesis method and characterized by series physical chemical assays. The acute full-thickness skin excision wound mouse model was used to access the wound healing potential and screen out the effective materials—Pd Icos NPs. Next evaluate the biotoxicity and safety of Pd Icos NPs and both in HaCaT cells and in vivo. Further examine related molecules expression by RT-qPCR and WB in HaCaT cells and wound tissues with Pd Icos treatment. Then knockout the related molecules both in HaCaT cells and in vivo to validate the molecular mechanism of these molecules in the phenotype of wound healing promoted by Pd Icos NPs.

**Results:** Pd Icos NPs with surface and tensile strain rather than Pd Oct NPs can promote skin wound healing. Pd Icos NPs upregulates the expression of HBEGF by promoting the production of transcription factor SP1, and contributes to keratinocytes proliferation and accelerating acute full-thickness skin wound healing.

**Discussion:** Pd Icos NPs represent an effective and safe material for skin wound healing, suggesting a potential novel therapeutic strategy.

**Keywords:** palladium icosahedral nanoparticles, keratinocytes, cell proliferation, skin wound healing, HBEGF, transcription factor SP1

## Introduction

The skin is the largest organ in the human body and serves as the main protector against the external environment. However, skin injury disrupts this physical barrier, resulting in loss of body fluids and nutrients, secondary bacterial infection, and disturbance of the internal environment of the body, which may cause life-threatening in severe cases.[1] Wound healing is a highly organized and complex process.[2] Various cells and bioactive substances play a critical role in inflammatory regulation, epidermal regeneration, angiogenesis, collagen synthesis, etc.[3] Of note, keratinocyte plays a key role in skin immune responses and epidermal barrier reconstruction. In response to the injury, keratinocytes are the first cells to be activated.[4] Immune cells are next recruited into the injury site and promote the wound healing process into the inflammatory stage. Cell proliferation is a necessary phase of wound



Received: 4 October 2024
Accepted: 28 February 2025
Published: 12 March 2025

healing. Keratinocytes proliferate in the basal layer, differentiate upward, and migrate to the center of the wound, which is responsible for wound closure.[5,6] The current treatment strategies are mainly to optimize these controllable related factors, such as clearing the infection, smoking cessation, nutritional support, etc. However, effective treatment is still lacking.[7] For the United States, accumulating epidemiological evidence in recent years reveals that the problems of wound healing impose a tremendous and rapidly increasing health and economic burden on patients and society.[8] Thus, it is necessary to develop more effective and targeted treatments for promoting wound healing directly.

Nanomaterials have unique physicochemical properties and can provide treatment at a molecular level, bringing new opportunities for medicine.[9–11] Noble metal nanoparticles attracted a great deal of scientific interest due to the higher catalytic activity and reaction selectivity as a result of their special features including large specific surface and surface energy, gold and silver are the most extensively studied materials[12] that have the ability to promote wound healing, but the price and cytotoxicity[13,14] seriously limit their clinical application. Palladium (Pd) exhibits superior catalytic performance and has been a critical subject for a wide range of applications such as electrocatalysis, energy storage and batteries, hydrogen storage systems, etc.[15] Conversely, the medical field research on Pd is still very limited. Only recently, researchers have noticed their potential therapeutic properties in anticancer therapy, thermal therapies, antibacterial therapy, and target delivery of drugs or genes.[16] Previous reports have demonstrated that Pd NPs are biologically inert and therefore exhibit low toxicity,[17] and might be a promising new material in the nanomedical field. However, these researches are based mostly on round-shaped Pd NPs. It has been found that the nanoparticles are within similar chemical properties, but different shapes can influence the efficacy of such materials in biological process.[18] Palladium octahedral nanoparticles (Pd Oct NPs) and palladium icosahedral nanoparticles (Pd Icos NPs) with {111} facets were reported to have greater catalytic activity compared to the other shapes.[19,20] Pd Oct NPs could pass through the bacterial membrane, thus can kill Gram-negative bacteria. Still, there was a lack of in vivo verification and its biological role in wound healing remains unclear. Moreover, the biological function of Pd Icos NPs have not been studied and reported yet. Here, we prepared and characterized the Pd Oct NPs and Pd Icos NPs of similar size and same crystal face, investigated their effect on the healing of acute full-thickness skin wounds and screened out the effective materials. Then we aim to clarify the biosafety and underlying molecular mechanism of the material in promoting wound healing and provide a new strategy for the clinic.

# Experimental

## Chemicals and Materials

Sodium tetrachloropalladate (II) ($Na_2PdCl_4$), polyvinylpyrrolidone (PVP, MW≈55,000) were purchased from Sigma-Aldrich. Diethylene glycol (DEG), potassium chloride (KCl) potassium bromide (KBr,), ascorbic acid (AA), acetone ($C_3H_6O$) and formaldehyde solution (HCHO, 37~40% in $H_2O$) were purchased from Sinopharm Chemical Reagent Co. Ltd (Shanghai, China). Ultrapure water (18.2 MΩ·cm) was used throughout the experiments. Synthesis of Pd nanocubes, Pd Oct NPs and Pd Icos NPs, production of blank gel were in Supporting Information 1.

## Synthesis of Pd Nanocubes

The Pd nanocubes were prepared according to previous work. First, 8.0 mL of an aqueous solution containing 105 mg of PVP, 60 mg of AA, 185 mg KCl, and 5 mg of KBr was hosted in a 30 mL vial and pre-heated to 80 °C in an oil bath under magnetic stirring for 10 min. Subsequently, 3.0 mL of an aqueous solution containing 57 mg of $Na_2PdCl_4$ was quickly injected with a pipette. After the vial had been capped, the reaction was then continued for 3 h. Pd nanocubes of roughly 6 nm in size were obtained. The product was collected by centrifugation, washed 5 times with water and acetone, and redispersed in 11mL $ddH_2O$ for further use.

## Synthesis of Pd Oct NPs

The Pd Oct NPs were synthesized according to the previously described method with slight modifications. In a typical synthesis, 105 mg of PVP, 100 μL of HCHO, 0.3 mL the as-prepared Pd nanocubes and 7.7 mL of $ddH_2O$ were mixed together in a 30 mL vial and pre-heated at 60 °C for 10 min under magnetic stirring. Subsequently, 3.0 mL of an aqueous

solution containing 29 mg of $Na_2PdCl_4$ was added to the pre-heated solution. After the vial had been capped, the reaction was then continued for 3 h. was collected by centrifugation, washed 3 times with water, and redispersed in $ddH_2O$ for further use.

## Synthesis of Pd Icos NPs

The Pd Icos NPs were synthesized according to the previously reported method with slight modifications. In a typical synthesis, 2 mL diethylene glycol and 105 mg PVP were added in a 30 mL vial, and pre-heated at 120 °C in an oil bath under magnetic stirring for 10 min. Subsequently, add 1.0 mL diethylene glycol containing 15.5mg $Na_2PdCl_4$ was injected using a pipette. After the vial had been capped, the reaction was then continued for 6 h. The product was collected by centrifugation and washed once with acetone and twice with water to remove excess PVP The product was finally redispersed in 3 mL $ddH_2O$ for further use.

## Production of Blank Gel, Pd Oct-Gel and Pd Icos-Gel

Polyacrylate Crosspolymer-6 (SEPIMAX ZEN) was purchased from SEPIC (France). Put 120 mg SEPIMAX ZEN powder into 8 mL $ddH_2O$, Pd Oct or Pd Icos suspension respectively, dispersed by ultrasonic waves and stirred at rate of 900 rpm overnight to prepared homogeneous blank-gel, Pd Oct-gel and Pd Icos-gel. The concentration of each gel was 0.65 mg/mL.

## Characterization of Materials

Structural and size analyses of the nanoparticles were performed using TEM (Hitachi HT7650 microscope) operated at 100 kV. HAADF-STEM images were collected on a JEOL ARM-200F field-emission transmission electron microscope operating at 200 kV accelerating voltage. XRD data was measured at BL14B station of Shanghai Synchrotron Radiation Facility (SSRF) and the used X-ray photon energy is 18 keV. Zeiss Sigma 300 SEM equipped with Smartedx energy dispersive spectrometer (Carl Zeiss AG, Germany) was used to observe the microstructure and elemental constitutions of gels. The hydrodynamic size and zeta potential were determined by DLS analyzer (Zetasizer Nano series, Malvern, UK).

## Cell Lines and Culture

HaCaT cells, NIH/3T3 cells, and HEK 293T cells were purchased from the American Type Culture Collection (ATCC; Manassas, VA, USA) and were cultured in Dulbecco's modified Eagle medium (DMEM; Gibco) supplemented with 10% fetal bovine serum (FBS; Gibco) at 37°C in 5%$CO_2$. The details of cytotoxicity and cell viability assay, cell proliferation analysis, quantitative real-time polymerase chain reaction, Western blot assays were in Supporting Information 1. The sequences of the primers are listed in Table S1.

## Animals and Treatments

C57BL/6J mice (7 weeks old) weighing between 20 and 25 g, were obtained from Shanghai SLAC Laboratory Animal Co. LTD (Shanghai, China). After initially anaesthetized, the hair on the back was shaved using an electric shaver. Further, mouse backs were cut to generate a circular full-thickness wound (diameter 0.6 cm) with a hole punch. Blank-gel, Pd Oct-gel and Pd Icos-gel were placed on the whole wound. The progression of wound closure was photographed monitored carefully every day, and the wound size was analyzed using ImageJ. The details of histological and immunofluorescent staining, hemolysis test was in Supporting Information 1. All animal experiments were performed under specific pathogen-free conditions and the experimental protocol was approved by the Animal Ethics Committee of the Xiangya Hospital of Central South University (2022020051). The study adhered to the guidelines set by the committee. The ethical principles outlined the Chinese National Guidelines (GB/T 35892-20181), Guide for the Care and Use of Laboratory Animals and other guidelines and laws related to animal welfare ethics were followed.

## Statistical Analysis

Data were presented as mean+SEM. The comparison between the two groups was performed by unpaired *t*-test, and the comparison between multiple groups was performed by one-way ANOVA along with Bonferroni's test. All statistical analysis was performed using GraphPad 9.0. Data were considered to be statistically significant if $P<0.05$.

# Results

## Characterization of Pd Oct NPs and Pd Icos NPs

The Pd Oct NPs and Pd Icos NPs with similar size were prepared according to a previously reported solution-phase synthesis based on aqueous solution or diethylene glycol using polyvinyl pyrrolidone (PVP) as the capping agent (Figure 1A).[21,22] The representative transmission electron microscopy (TEM) images and the size distribution statistical results showed that the Pd Oct NPs and Pd Icos NPs have a single morphology and similar average size of about 15nm (Figure 1B and C). Both the octahedron and icosahedron were enclosed by {111} facets, and the icosahedron is an assembly of twenty tetrahedral single-crystallites with thirty twin boundaries, which could be clearly observed by the atomic-resolution high-angle annular dark-field scanning TEM (HAADF-STEM) images in Figure 1D and E. The average {111} spacing of single Pd Oct (Figure 1D and E) was calculated to be 2.26 Å, consistent with the value of single-crystalline bulk (2.25 Å), while the average {111} spacing at the central faces for the Pd Icos was measured to be 2.32 Å (Figure 1F), slightly larger than the Pd Oct. This result reveals the surface of Pd Icos is in tensile strain. The X-ray diffraction (XRD) pattern presented the peaks of Pd icosahedra slightly shifted to a lower diffraction angle compared with Pd octahedra (Figure 1G), indicating a large lattice constant of Pd icosahedra. Besides, the {111} diffraction peak of Pd icosahedra presented a small hump at a high angle, implying that the distribution of surface strain on the icosahedra was not uniform.[23] All these preceding characterizations and analyses thus have demonstrated the existence of surface tensile strain on the icosahedra and a negligible strain on the octahedra. In addition, the aqueous solutions containing Pd Oct NPs and Pd Icos NPs respectively were subjected to dynamic light scattering (DLS) tests and Zeta potential measurements (Figure 1H and I). Figure 1H showed that the hydrodynamic diameter of Pd Oct and Pd Icos was 107.6 nm and 87.08 nm. The mean zeta potential values of Pd Oct and Pd Icos were −0.995 mV and −8.78 mV (Figure 1I), indicating that Pd Icos is more stable and much better dispersed than Pd Oct in aqueous solution.

Since the aqueous solution has high fluidity which is not suitable for subsequent animal experiments by external application. We use SEPIMAX ZEN as gel formulation matrix.

SEPIMAX ZEN has excellent characteristics of low skin irritation, excellent biocompatibility, superior suspension stability, ease of gel preparation, broad pH range applicability and precise viscosity adjustment. It has been widely used in the cosmetics and personal care industry. We then prepared and characterized the SEPIMAX ZEN gel (blank-gel), Pd Octahedra-gel (Pd Oct-gel) and Pd Icosahedra-gel (Pd Icos-gel). The colors of both particles in the gel were dark brown (Figure 2A). Figure 2B showed the scanning electron microscope (SEM) images of these gel. Compared with the blank-gel, the surface of Pd Oct-gel and Pd Icos-gel became rough and granular, suggesting the incorporation of Pd nanoparticles. We then analyzed the composition of different gels and further confirmed that Pd Oct NPs and Pd Icos NPs were successfully embedded in SEPIMAX ZEN gel by energy-dispersive X-ray spectrometry (EDS) (Figure 2C). TEM results showed that Pd Oct NPs and Pd Icos NPs did not have morphological changes or obvious aggregation in gel (Figure 2D) and the average particle sizes remained around 15 nm (Figure 2E). Three gels were dissolved in deionized water and subjected to DLS analysis. The results showed that the mean zeta potential values of blank-gel, Pd Oct-gel and Pd Icos-gel were −28.8 mV, −51.9 mV and −26mV, respectively (Figure 2F), indicating that Pd Oct-gel is much better dispersed and more stable than blank-gel or Pd Icos-gel in aqueous solution. However, there is no obvious difference between blank-gel and Pd Icos-gel. Zeta potential can reflect the relative stability of materials under different formulation compositions. Along one months of storage, no changes such as edimentation or sedimentation was observed in three gels. In order to reduce the impact of this difference, we only use freshly prepared gels in each experiment.

## Pd Icos-Gel Accelerates the Full-Thickness Skin Wound Healing Process

To explore the therapeutic effect of Pd Oct-gel and Pd Icos-gel on the healing of acute skin wounds and screen out the effective materials, full-thickness skin wounds on the back of the mice were created and treated with blank-gel, Pd Oct-gel and Pd Icos-gel (Figure S1). Representative images of the wound closures on post-surgery days 0 to 6 were exhibited (Figure 3A). The wound healing rate was shown in Figure 3B. The digital photos of the wounds and quantification of the closure rates at days 2 to 5 after wounding revealed that the topical application of Pd Icos-gel markedly accelerated the

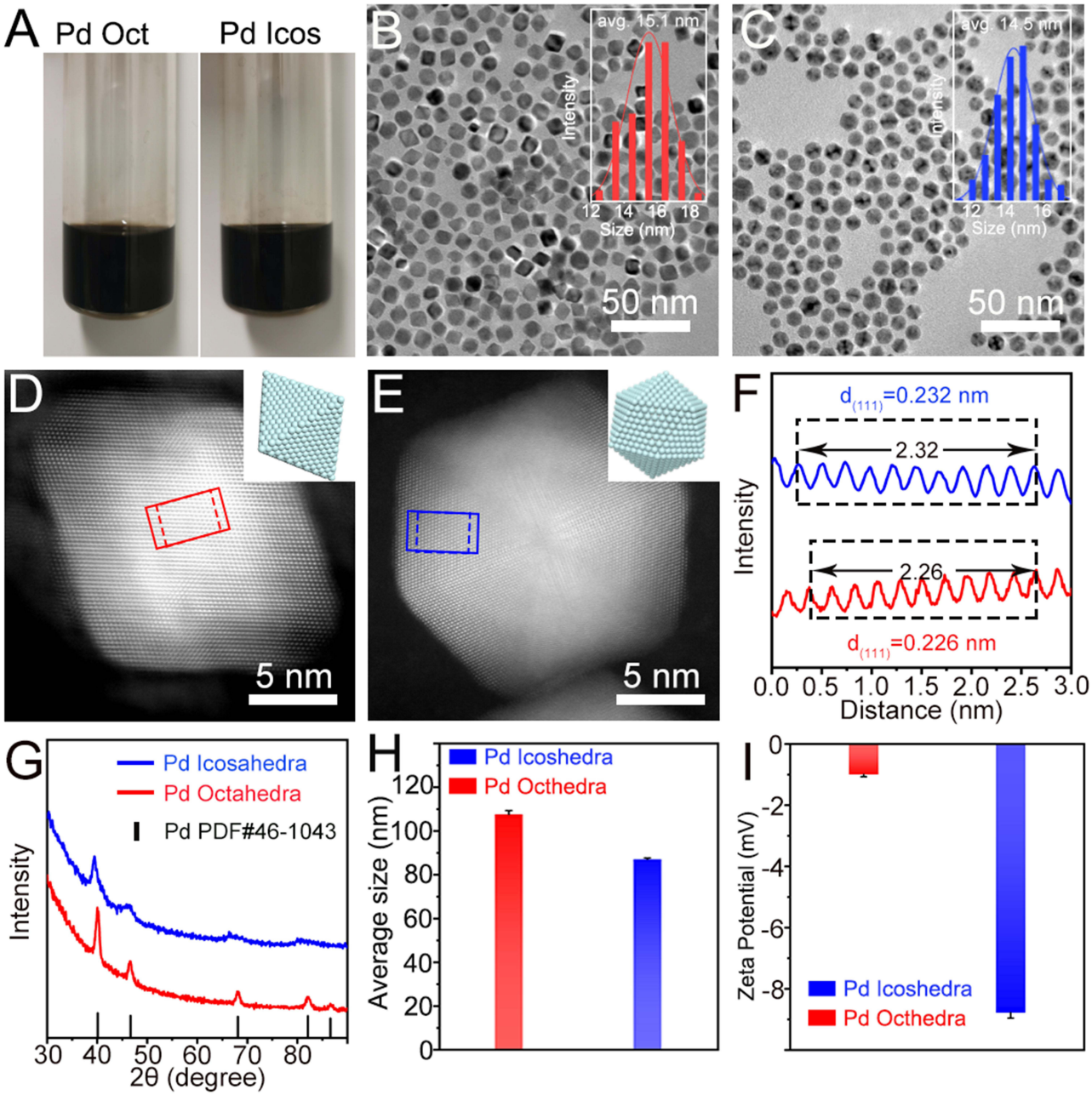


**Figure 1** Characterization of Pd Oct NPs and Pd Icos NPs. (**A**) Digital photos of Pd Pct and Pd Icos NPs aqueous solution. (**B** and **C**) TEM images of Pd Pct (**B**) and Pd Icos NPs (**C**). The inset shows the size distribution by counting more than 200 individual nanocrystals. Scale bar: 50nm. (**D** and **E**) HADDF-TEM image of an individual particle of Pd Oct NPs and Pd Icos NPs. The inset shows corresponding models of the nanostructures. Scale bar: 5nm. (**F**) The intensity profiles taken from the regions boxed by red and blue rectangles in (**D** and **E**), respectively. (**G**) XRD of Pd Oct NPs and Pd Icos NPs. (**H**) DLS measurements for hydrodynamic diameter of Pd Oct NPs and Pd Icos NPs. (**I**) Zeta potentials of Pd Oct NPs and Pd Icos NPs tested by DLS analysis.

wound closure of wounds compared with the blank-gel, whereas the Pd Oct-gel-treated group showed no statistically significant difference.

Next, we further explored the biological effects of Pd Icos NPs on wound tissues. Hematoxylin and eosin (H&E) staining results verified that wound closure occurred more rapidly in the Pd Icos-gel group than control (Figure 3C). As seen in representative pictures and statistical results, compared with blank-gel, the regenerated epidermal thickness around the wound edge in the Pd Icos-gel group was thicker than the control at day 2 to 4 post-treatment (Figure 3D), indicating that Pd Icos-gel may promote keratinocytes proliferation. To confirm this effect, immunofluorescence double


https://doi.org/10.2147/IJN.S499289

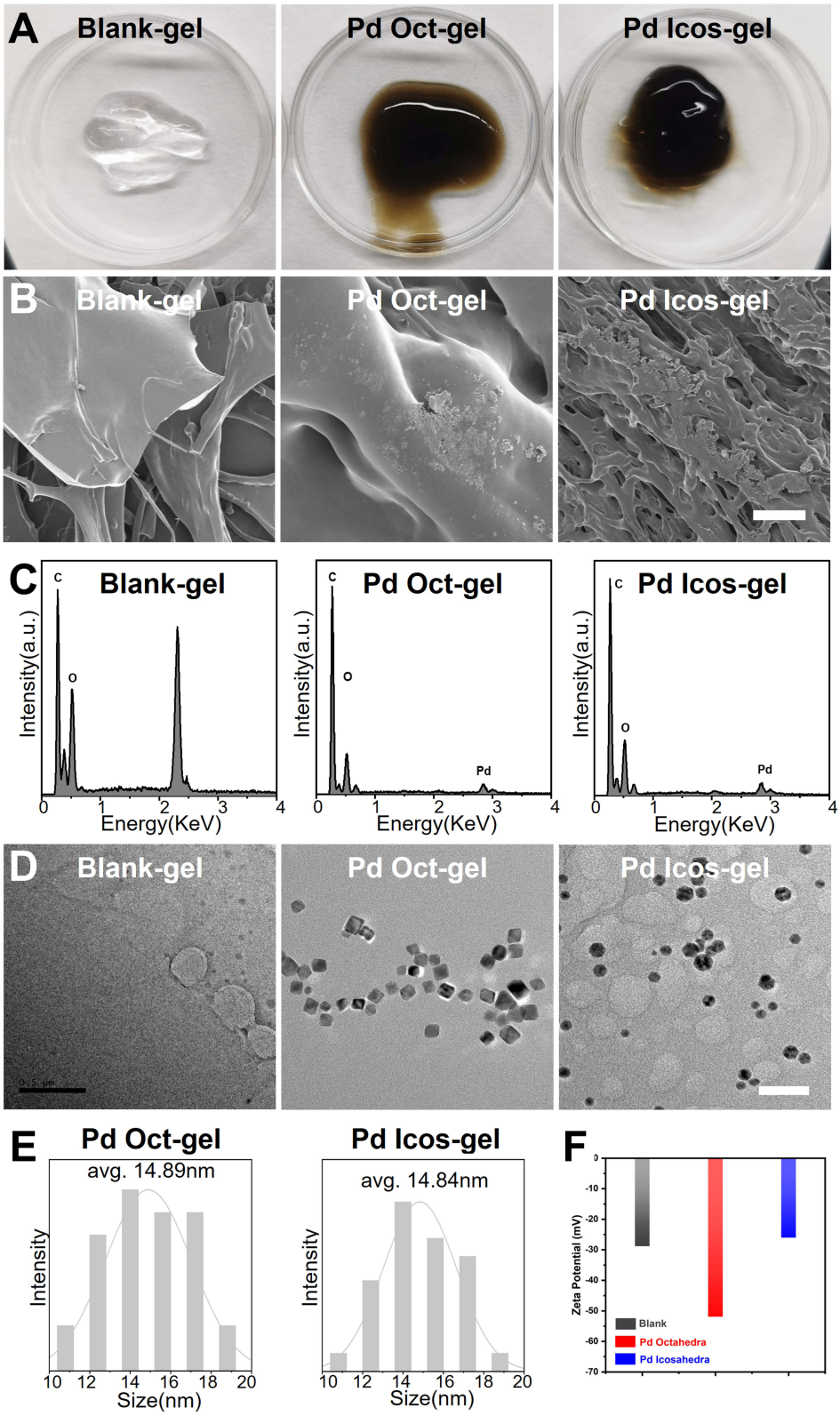


**Figure 2** Characterization of blank-gel, Pd Oct-gel and Pd Icos-gel. (**A**) Representative images of blank-gel, Pd Oct-gel and Pd Icos-gel. (**B**) SEM images of blank-gel, Pd Oct-gel and Pd Icos-gel. Scale bar: 20μm. (**C**) EDS spectra of blank-gel, Pd Oct-gel and Pd Icos-gel. (**D**) TEM images of blank-gel, Pd Oct-gel and Pd Icos-gel. Scale bar: 50nm. (**E**) The size distribution of Pd Oct and Pd Icos in gel calculated from TEM images. (**F**) Zeta potentials of blank-gel, Pd Oct-gel tested by DLS.

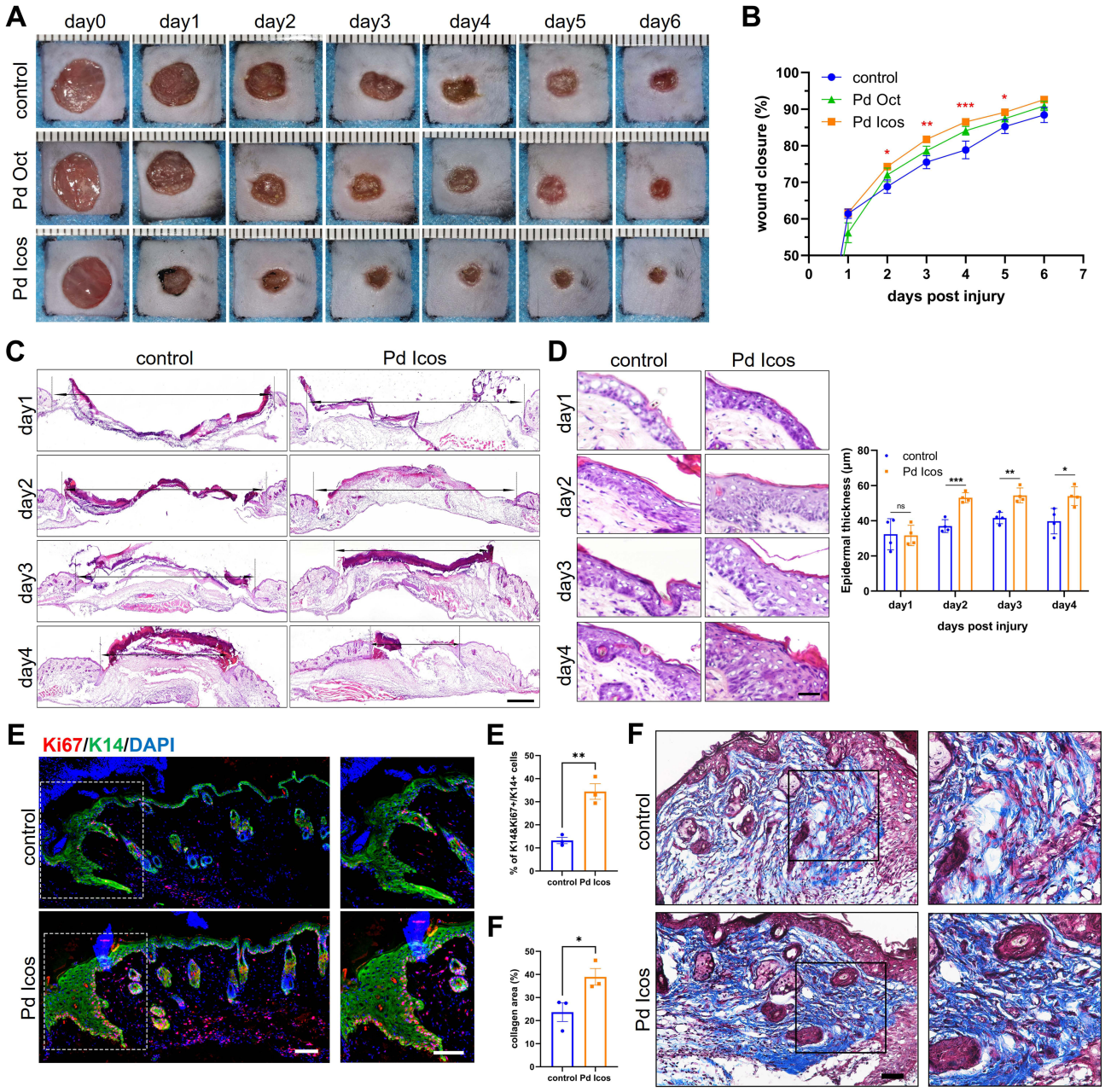


**Figure 3** Pd Icos-gel accelerates the healing of full-thickness skin wounds. (**A**) Gross view of wounds from mice treated with blank-gel (control), Pd Oct-gel or Pd Icos-gel at the indicated time points. (**B**) The rate of wound closure (n=4). (**C**) Representative H&E stained images of wounds. Double-headed arrows indicate the scars. Scale bar: 200μm. (**D**) Representative H&E stained wound edge show epidermal thickness of at the indicated time points. Quantified data of the average epidermal thickness were calculated in H&E staining (n = 4). (**E**) Immunofluorescence staining images for Ki67 (red) and K14 (green) in wounds and ratio of the Ki67+/K14+ cells on day 4 (n=3). Scale bar: 100μm. (**F**) Masson's trichrome staining images of wounds and quantification of the average intensity for Masson-stained areas (n=3). Scale bar: 100μm. The comparison between the two groups was performed by unpaired *t*-test, and the comparison between multiple groups was performed by one-way ANOVA. Data are presented as means ± SEM (ns means P>0.05, *P<0.05, **P<0.01, ***P<0.001).

staining was performed for proliferative marker Ki67 and keratinocytes marker K14 on day 4 (Figure 3E). Consistently, a much larger number of Ki67+K14+ cells were observed in the Pd Icos-gel group than in the control group. Meanwhile, the wounds treated with Pd Icos-gel also had markedly higher extents of collagen deposition compared with the wounds receiving blank-gel treatments, as indicated by Masson's trichrome staining (Figure 3F). All the above results strongly demonstrate that Pd Icos-gel could effectively promote cell proliferation, especially for keratinocytes, thus facilitating wound tissue repair.


https://doi.org/10.2147/IJN.S499289

Epidermis forms the outermost layer and barrier of the skin. As previously shown, nanoparticles can penetrate the stratum corneum easier, and cross the skin barrier.[24] We wondered which layer of the skin Pd Icos NPs can penetrate, accumulate and play a role in wound healing. So, we collect the wound tissue after Pd Icos-gel was treated for 6 days and analyzed by using TEM. The incorporation of Pd Icos nanomaterials can be seen in TEM images (Figure S2). Pd Icos nanomaterials of various sizes were found accumulating in the cytoplasm, vesicles, and numerous mitochondria of keratinocytes in the basal layer and spinous layer. This indicates that the Pd Icos nanomaterials can penetrate deeply into the cells of the epidermal basal layer. The details of biocompatibility and safety of Pd Icos nanomaterials were shown in Figure S3.

## Pd Icos NPs Promote the Cellular Proliferation of HaCaT Cells

Our in vivo studies have shown that the Pd Icos NPs can effectively promote the proliferation of keratinocytes around the wound. Therefore, the biological activity of Pd Icos NPs on HaCaT cell proliferation was then examined. As shown in Figure 4A, the cell proliferation curve indicated that 2.5μg/mL of Pd Icos NPs significantly promoted the proliferation of HaCaT cells after 36h and 60h cultures compared with the controls. Then, we further explored the cell proliferation process by the Edu fluorescence staining method. As shown in Figure 4B, Pd Icos NPs (2.5μg/mL) increased the positive rate of Edu staining compared with the control. Similarly, the colonies formed assay showed a significant increase in the number of colonies formed in the Pd Icos NPs treated group (Figure 4C). Previous studies showed AKT and STAT3 signaling pathway activation contribute to the proliferation of keratinocytes and skin wound regeneration.[25,26] Thus, we wanted to investigate whether they were stimulated by the Pd Icos NPs treatment of HaCaT cells. Accordingly, the STAT3 activation (p-STAT3) and the AKT activation (p-AKT) were significantly upregulated by stimulating with Pd Icos NPs (Figure 4D). Together, our findings showed Pd Icos NPs can directly promote keratinocyte proliferation, which is an important factor in wound healing.

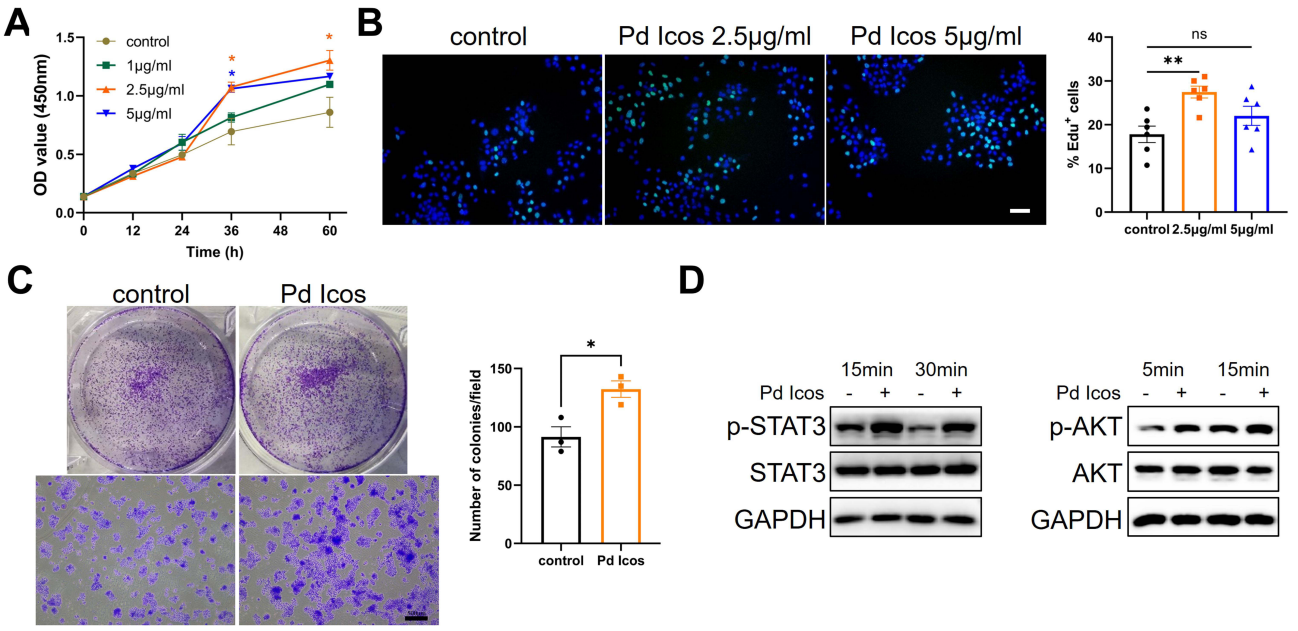


**Figure 4** Pd Icos NPs promotes the proliferation of HaCaT cells. (**A**) The proliferation of HaCaT cells was assessed by CCK-8 assays. HaCaT cells were separately incubated with different doses (0, 1, 2.5, 5μg/mL) of Pd Icos NPs for 12–60 hours. (**B**) Immunofluorescence staining of EdU incorporation into nuclei. HaCaT cells were treated with different doses (0, 2.5, 5μg/mL) of Pd Icos NPs for 36 hours. The Edu incorporation rate was shown as the ratio of Edu positive cells (green) to total Hoechst33342 positive cells (blue). Scale bar: 200μm. (**C**) Representative images and quantification of colonies formed by HaCaT cells treated with 2.5μg/mL Pd Icos NPs for 7 days. Scale bar: 500μm. (**D**) Pd Icos NPs induced STAT3 and AKT signaling activation. Sub-confluent HaCaT cells were starved for 12 hours and afterward treated with 2.5μg/mL Pd Icos NPs for 5 to 30 minutes. Phosphorylated STAT3 (pSTAT3) and phosphorylated AKT (pAKT) levels were detected by immunoblotting. These data represent three separate experiments. The comparison between the two groups was performed by unpaired *t*-test, and the comparison between multiple groups was performed by one-way ANOVA or two-way ANOVA. Data are presented as means ± SEM (ns means P>0.05, *P<0.05, **P<0.01).

 https://doi.org/10.2147/IJN.S499289 

## Pd Icos NPs Promote Keratinocyte Proliferation and Wound Healing Through HBEGF

To further explore the molecular mechanism of Pd Icos NPs regulating keratinocytes proliferation and wound healing, we first systematically screened a series of major growth factors and inflammatory factors affecting the proliferation of keratinocytes and wound healing by detecting their mRNA levels in HaCaT cells and wound tissues treated with Pd Icos NPs.[27,28] The results showed that incubation with Pd Icos NPs obviously increased the expression of *HBEGF*, beta fibroblast growth factor (*bFGF*), and transformation growth factor- β (*TGF-β)* compared to control in HaCaT cells (Figures 5A and S4). Meanwhile, the mRNA levels of Hbegf were significantly increased in wound tissues treated with Pd Icos NPs on days 1 to 6 after injury compared with the blank-gel treatment group, while the other growth factors did hardly changed (Figures 6A and S5). To further support our observations, the protein levels of HBEGF in HaCaT cells and wound tissues were detected. As the result shown in Figures 5B and 6B, both in vitro and in vivo, HBEGF protein levels were upregulated by Pd Icos NPs.

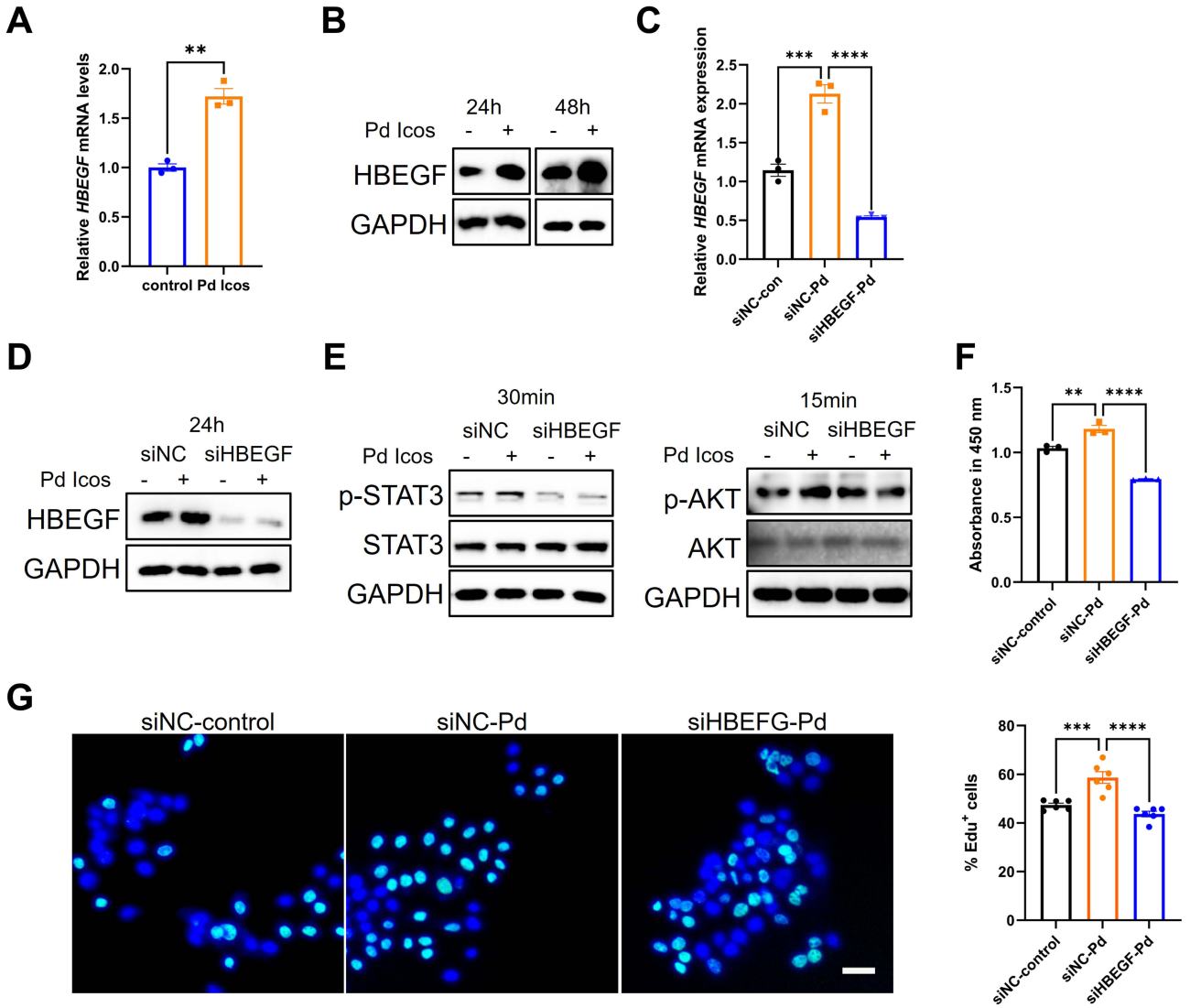


**Figure 5** HBEGF expression is increased in HaCaT cells induced by Pd Icos NPs. (**A**) The mRNA levels of HBEGF in HaCaT cells induced by Pd Icos NPs for 2h. (**B**) The protein level of HBEGF in HaCaT cells induced by Pd Icos NPs for 24h and 48h. (**C**–**G**) HaCaT cells with HBEGF knocked down were treated with Pd Icos NPs. RT-qPCR analysis showing the mRNA levels of HBEGF (2h) (**C**), Western blot analysis showing the expression of HBEGF (**D**), p-STAT3 and p-AKT (**E**), CCK-8 assay (**F**) and immunofluorescence staining of EdU (**G**) showing the effects of silenced HBEGF on cell proliferation induced by Pd Icos NPs. Scale bar: 50μm. GAPDH is the loading control. – indicates control group, + indicates 2.5μg/mL Pd Icos NPs treatment group. siNC: negative control group, siHBEGF: HBEGF-knockdown group. These data represent three separate experiments. The comparison between the two groups was performed by unpaired *t*-test, and the comparison between multiple groups was performed by one-way ANOVA. Data are presented as means ± SEM. ns means P>0.05, **P<0.01, ***P<0.001, ****P<0.0001.


https://doi.org/10.2147/IJN.S499289

Therefore, we speculate that HBEGF could be regulated or act as the target molecule regulated by Pd Icos NPs. As shown in Figure 5C–E, HBEGF deficiency inhibited HBEGF expression and activation of AKT and STAT3 signaling pathways induced by Pd Icos NPs. In addition, evidentially, the CCK-8 assay demonstrated that silencing HBEGF showed decreased keratinocyte proliferation in the Pd Icos NPs-treated group (Figure 5F), and the Edu proliferation assay showed similar results (Figure 5G). These results suggested that the HaCaT cell proliferation induced by Pd Icos NPs was significantly inhibited by HEBGF knockout in vitro. To validate the regulatory mechanism of HBEGF in the wound healing promoted by Pd Icos NPs, local cutaneous HBEGF knockdown with acute full-thickness skin excision wound mouse model was constructed by intradermal injection of shRNA and further treated by Pd Icos-gel (Figure S6). Initially, we confirmed both at the mRNA and protein level that indeed HBEGF is downregulated. Consistent with our findings in vitro, the expression of HBEGF in the Pd Icos-treated shHBEGF group was significantly lower than the control group (Figure 6C and D). Subsequently, we monitor the general situation of the wound and analyze the wound healing rate. HBEGF knockdown could attenuate the accelerated wound healing process induced by Pd Icos gel (Figure 6E–H). Together, Pd Icos NPs could facilitate keratinocyte proliferation by inducing HBEGF expression, which contributes to accelerating skin wound healing.

## The Promotion of HBEGF Expression by Pd Icos NPs Depends on SP1

Next, we sought to illustrate how Pd Icos NPs regulate the expression of HBEGF. According to the above results, we speculated that the possible mechanisms underlying this process may be associated with the regulation of transcription factors (TFs) of HBEGF.[29,30] We first predicted five potential transcription factors of HBEGF by using reliable Transcription Factor datasets, including Cistrome DB, hTFtarget, ENCODE and humanTFDB. Venn diagram summarizing the overlap of candidate TFs predicted from different bioinformatics algorithms (Figure 7A). Of them, EP300 is known to be a cofactor that can complex with MYC and activate MYC.[31] Hence, we examined the expression of SP1, AP1, CTCF and MYC in Pd Icos NPs-treated HaCaT cells (Figure S7) and confirmed that Pd Icos only increased the expression of SP1 (Figure 7B).

We then investigated whether SP1 expression was essential in the process of Pd Icos NPs promoting HBEGF expression. We silenced SP1 by siRNA in HaCaT cells and treated them with Pd Icos NPs. The results confirmed that both the mRNA and protein levels of HBEGF were apparently increased by Pd Icos NPs and were significantly downregulated by SP1 knockdown (Figure 7C–E). Additionally, a CCK-8 assay was also performed and silencing SP1 indeed reversed the cell proliferation induced by Pd Icos NPs in HaCaT cells (Figure 7F). In conclusion, these results indicate that the promotion of HBEGF expression by Pd Icos NPs depends on SP1.

# Discussion

Recently, with the rapid advancement in nanotechnology, an increasing number of studies have reported that noble metal nanoparticles represent special biological properties and exhibit obvious performance advantages in biomedical applications.[32,33] Especially, researchers have paid particular attention to their benefits for application in wound healing. An extensive study has proposed that the size, morphology, surface ligands, or charge of metal nanoparticles play a significant role in their selectivity, catalytic activity, and reusability.[34,35] However, the specific impact of these parameters on the biological effects and therapeutic efficacy of medicine remains inconclusive.[36] Here, we revealed the much better pro–wound healing properties of Pd Icos-gel in vivo compared with Pd Oct-gel. Pd Oct {111} with lower surface energy has been reported to have higher antioxidant enzyme-like activities, and can protect cells from oxidative stress-induced damage. Another study revealed that the tensile strain on the surface of Pd icosahedra is beneficial to the formation of intermediates, leading to enhanced peroxidase-like activities than unstrained Pd Oct. This reminds us that the antioxidant capacity of metal nanoparticles may be related to their ability to promote wound healing. Some researchers found that doped metals (Au, Cu, Pd) on silver nanoparticles (Ag NPs) can improve the therapeutic effects on antibacterial and wound healing, whereas Pd−Ag NPs showed the best enhancement effect They considered this attributed to Pd could tune the d band center largest upshift toward the Fermi level.[37] Previous studies have clearly that Pd icosahedra have a distinct tensile strain and upward shift of the d-band center of the surface atom mainly by the combination of molecular dynamics (MD) simulations and density functional theory (DFT) calculations.[21,22] Our

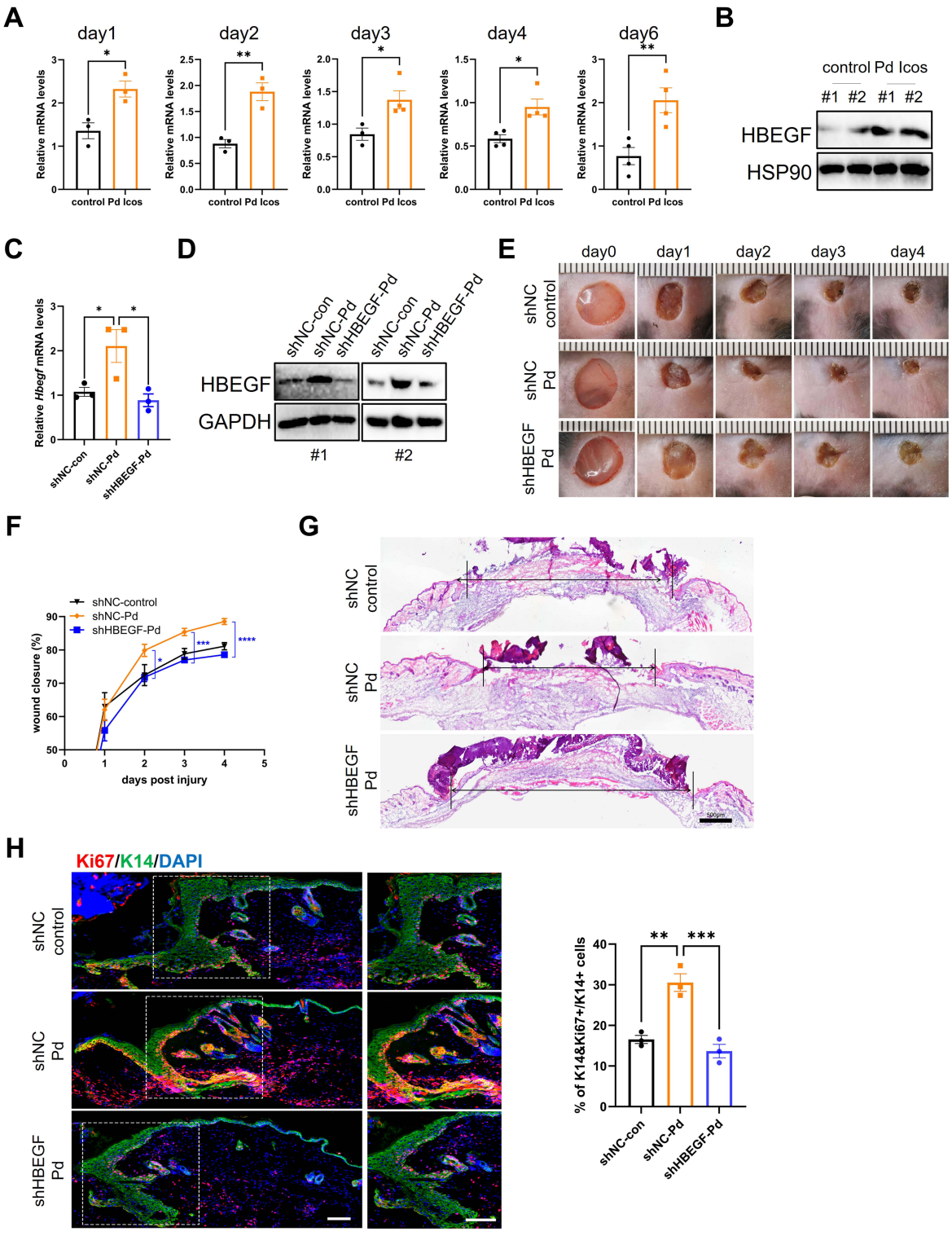


**Figure 6** HBEGF deficiency reverses the wounds healing promotion induced by Pd Icos-gel. (**A**) RT-qPCR analysis showing the mRNA levels of *Hbegf* in vivo treated with Pd Icos-gel for different days (n≥3 per group). (**B**) Western blot analysis of HBEGF expression of wound tissue treated with Pd Icos-gel for 4 days. (**C**–**F**) Local cutaneous *Hbegf* knockdown with full-thickness skin wounds mice were treated with Pd Icos NPs (n≥3 per group). The mRNA levels of HBEGF (**C**) and the protein level of HBEGF (**D**) in wound tissue on day4. The mRNA levels of HBEGF (**E**) and the protein level of HBEGF (**F**) in wound tissue on day 4. HSP90 or GAPDH is the loading control. #1 and #2 represent different group. The gross view of wounds (**E**) from mice treated with blank-gel (control) or Pd Icos-gel (Pd) at the indicated time points and the rate of wound closure (**F**) (n=4). (**G**) Representative H&E-stained images of wounds. (**H**) Immunofluorescence staining images for Ki67 (red) and K14 (green) in wounds and ratio of the $Ki67^{+}/K14^{+}$ cells on day 4 (n=3). Scale bar: 100μm. Double-headed arrows indicate the scars. Scale bar: 500μm. shNC: negative control group, shHBEGF: HBEGF-knockdown group. These data represent three separate experiments. The comparison between the two groups was performed by unpaired *t*-test, and the comparison between multiple groups was performed by one-way ANOVA. Data are presented as means ± SEM. ns means P>0.05, *P<0.05, **P<0.01, ***P<0.001, ****P<0.0001.


https://doi.org/10.2147/IJN.S499289

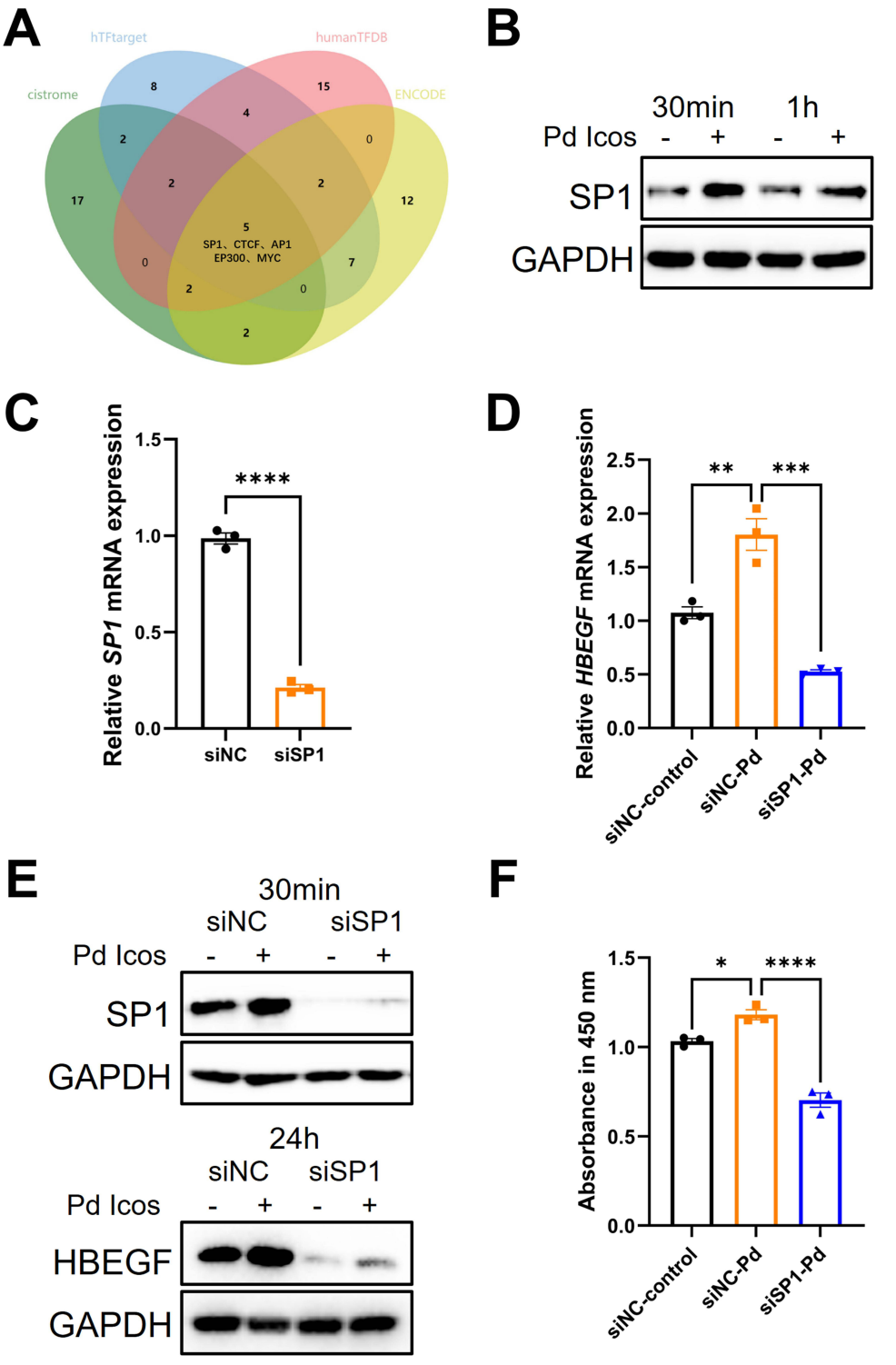


**Figure 7** Pd Icos NPs upregulate the levels of HBEGF by enhancing SP1 expression. (**A**) Venn diagram summarizing the candidate transcription factors predicted from four different bioinformatics algorithms. (**B**) The protein level of SP1 in HaCaT cells induced by Pd Icos NPs for 30min or 1h. (**C**) The mRNA level of SP1 expression in HaCaT cells after knockdown of SP1. (**D** and **E**) HaCaT cells with SP1 knocked down were treated with Pd Icos NPs. RT-qPCR analysis showing the mRNA levels of HBEGF (2h) (**D**), Western blot analysis showing the expression of SP1 (30min) and HBEGF (24h) (**E**). (**F**) CCK-8 assay showed the effects of silenced SP1 on cell proliferation induced by Pd Icos NPs. GAPDH is the loading control. –indicates control group, +indicates 2.5μg/mL Pd Icos NPs treatment group. siNC: negative control group, siSP1: SP1-knockdown group. Data are representative of at least 3 independent experiments and are shown as mean ± SEM. The comparison between the two groups was performed by unpaired *t*-test, and the comparison between multiple groups was performed by one-way ANOVA. ns means P>0.05, *P<0.05, **P<0.01, ***P<0.001, ****P<0.0001.

characterization results came to a similar conclusion in line with these earlier findings. Hence, we speculate this may also be the reason for the superior performance of Pd Icos NPs than Pd Oct NPs. Although there is no definite conclusion and requires further investigation, it is reminded that the surface strain or d-band center can also be used as an important knob to design and tune the biological function of nanomaterials.

Previous research has mainly focused on the ability of these noble metal-based nanoparticles to catalyze the generation of reactive oxygen species (ROS) and inhibit or kill bacteria in infected wounds. But in this research, we pay more attention to whether they are possible to promote wound healing directly. Although keratinocytes proliferation and wound healing are controlled by a wide variety of growth factors, cytokines and chemokines, we only detected an increase in HBEGF after Pd Icos treatment. HBEGF is a transmembrane hydrolyzed protein that is first synthesized in a membrane-anchored form (pro-HBEGF), and then shed into extracellular s-HBEGF and intracellular c-HBEGF structure. Previous studies revealed that the function of HBEGF is related to the quantity of pro-HBEGF, which is a strict and complex regulation process.[38] Early studies noted that the secretion of HBEGF in wound keratocytes reached a maximum on days 2–3 and disappeared around 6 days.[39] Normally, the expression and interaction of HBEGF and EGFR in keratinocytes will not cause excessive proliferation on its own. After the skin is traumatized, autocrine expression of HBEGF increased and activates EGFR, regulating cell proliferation, differentiation, and migration through a variety of cell signaling pathways including AKT and STAT3 pathway.[40] When the damaged epithelial layer was fully restored, the interaction of proHBEGF with EGFR returned to a balanced state.[41] Our study showed similar results that Pd Icos NPs can promote HBEGF expression and lead to keratinocyte proliferation and skin wound healing. Besides, our results show that wounds treated with Pd Icos-gel exhibited significantly higher levels of collagen deposition compared to controls at day 4 post-injury. However, both granulation tissue formation and collagen deposition were usually notably increased primarily at day 7 post-injury. More experiments are needed to assess the effect of Pd Icos on these processes during the wound healing. Moreover, studies have found that HBEGF could promote retinal angiogenesis, vascular smooth muscle cell,[42,43] and neuronal cell proliferation[44] in the form of paracrine secretion. This also suggests that Pd Icos NPs have the potential to promote angiogenesis and neural immigration in wound regeneration. However, depth research is required to speculate and confirm further whether Pd Icos NPs can directly modulate these wound healing–related biological processes.

SP1 is one of the most well-characterized transcriptional activators that control the activation of about 6000 genes. Its target genes are mainly involved in cell proliferation and oncogenesis.[45] Previously, studies have indicated that SP1 is a crucial transcription factor required for HBEGF expression.[46] Likewise, we found that SP1 mediated the facilitation of Pd Icos on HBEGF. Despite these findings, it remains unanswered the precise mechanism as to how PdNPs interact with SP1. Whether there may be other target genes or regulatory mechanisms, still requires more investigations. The specific physiological process of Pd Icos in cells and in vivo is also an interesting question to explore in future studies.

## Conclusions

Pd Icos NPs can accelerate the healing of acute full-thickness wounds and are superior to Pd Oct NPs. For the first time, we confirmed the therapeutic effect of Pd Icos NPs on skin wounds and elucidated its potential mechanism. In detail, Pd Icos NPs increase the HBEGF expression by upregulating its transcription factor SP1, which in turn promotes the keratinocytes proliferation through the activation of AKT and STAT3 pathways, and finally results in accelerating wound healing. Notably, our findings demonstrated that Pd Icos NPs had superior biocompatibility in both in vitro and in vivo experiments. Therefore, this work implied the promising prospect of Pd Icos NPs as a potential therapeutic candidate for skin wound healing.

## Data Sharing Statement

All data that support the findings of this study are available from the corresponding authors upon reasonable request.

## Ethics Approval Statement

All the experimental protocol was approved by the Animal Ethics Committee of the Xiangya Hospital of Central South University (2022020051).

## Author Contributions

All authors made a significant contribution to the work reported, whether that is in the conception, study design, execution, acquisition of data, analysis and interpretation, or in all these areas; took part in drafting, revising or critically reviewing the article; gave final approval of the version to be published; have agreed on the journal to which the article has been submitted; and agree to be accountable for all aspects of the work.

## Funding

This work was supported by the National Key Research and Development Program of China No.2021YFF1201200, National Natural Science Funds for Distinguished Young Scholars (grant nos. 82225039), National Natural Science Foundation of China (grant nos. 81974480), Natural Science Foundation of Hunan Province (grant nos. 2021JJ31098), China Postdoctoral Science Foundation funded project (grant nos. 2021T140752, 2021M693560).

## Disclosure

The authors declare that there is no conflict of interests in this work.

## References

1. Gurtner GC, Werner S, Barrandon Y, Longaker MT. Wound repair and regeneration. *Nature*. 2008;453:314–321. doi:10.1038/nature07039
2. Park S, Gonzalez DG, Guirao B, et al. Tissue-scale coordination of cellular behavior promotes epidermal wound repair in live mice. *Nat Cell Biol*. 2017;19:155. doi:10.1038/ncb3472
3. Barrientos S, Stojadinovic O, Golinko MS, et al. Growth factors and cytokines in wound healing. *Wound Repair Regener*. 2008;16:585–601. doi:10.1111/j.1524-475X.2008.00410.x
4. Jiang Y, Tsoi LC, Billi AC, et al. Cytokinocytes: the diverse contribution of keratinocytes to immune responses in skin. *JCI Insight*. 2020;5: e142067. doi:10.1172/jci.insight.142067
5. Avitabile S, Odorisio T, Madonna S, et al. Interleukin-22 promotes wound repair in diabetes by improving keratinocyte pro-healing functions. *J Invest Dermatol*. 2015;135:2862–2870. doi:10.1038/jid.2015.278
6. Paladini RD, Takahashi K, Bravo NS, et al. Onset of re-epithelialization after skin injury correlates with a reorganization of keratin filaments in wound edge keratinocytes: defining a potential role for keratin 16. *J Cell Biol*. 1996;132:381–397. doi:10.1083/jcb.132.3.381
7. Sun BK, Siprashvili Z, Khavari PA. Advances in skin grafting and treatment of cutaneous wounds. *Science*. 2014;346:941–945. doi:10.1126/science.1253836
8. Sen CK. Human wounds and its burden: an updated compendium of estimates. *Adv Wound Care*. 2019;8:39–48. doi:10.1089/wound.2019.0946
9. McNamara K, Tofail SAM. Nanosystems: the use of nanoalloys, metallic, bimetallic, and magnetic nanoparticles in biomedical applications. *Phys Chem Chem Phys*. 2015;17:27981–27995. doi:10.1039/C5CP00831J
10. Luan Q, Qiao R, Wu X, et al. Plant-derived Chinese herbal hydrogel microneedle patches for wound healing. *Small*. 2024;20(45):e2404850. doi:10.1002/smll.202404850
11. Song C, Wu X, Wang Y, Wang J, Zhao Y. Cuttlefish-inspired photo-responsive antibacterial microparticles with natural melanin nanoparticles spray. *Small*. 2024;20(19):e2310444. doi:10.1002/smll.202310444
12. Fadilah NIM, Isa ILM, Zaman WSWK, et al. The effect of nanoparticle-incorporated natural-based biomaterials towards cells on activated pathways: a systematic review. *Polymers*. 2022;14:476. doi:10.3390/polym14030476
13. Hammer B, Norskov JK. Why gold is the noblest of all the metals. *Nature*. 1995;376:238–240. doi:10.1038/376238a0
14. Salesa B, Assis M, Andrés J, et al. Carbon nanofibers versus silver nanoparticles: time-dependent cytotoxicity, proliferation, and gene expression. *Biomedicines*. 2021;9:1155. doi:10.3390/biomedicines9091155
15. Chen A, Ostrom C. Palladium-based nanomaterials: synthesis and electrochemical applications. *Chem Rev*. 2015;115:11999–12044. doi:10.1021/acs.chemrev.5b00324
16. Phan TTV, Huynh T-C, Manivasagan P, et al. An up-to-date review on biomedical applications of palladium nanoparticles. *Nanomaterials*. 2019;10:66. doi:10.3390/nano10010066
17. Ding L, Yao C, Yin X, et al. Size, shape, and protein corona determine cellular uptake and removal mechanisms of gold nanoparticles. *Small*. 2018;14:e1801451. doi:10.1002/smll.201801451
18. Ridolfo R, Tavakoli S, Junnuthula V, et al. Exploring the impact of morphology on the properties of biodegradable nanoparticles and their diffusion in complex biological medium. *Biomacromolecules*. 2021;22:126–133. doi:10.1021/acs.biomac.0c00726
19. Lim J, Liu C-Y, Park J, et al. Structure sensitivity of Pd facets for enhanced electrochemical nitrate reduction to ammonia. *ACS Catal*. 2021;11:7568–7577. doi:10.1021/acscatal.1c01413
20. Xi Z, Cheng X, Gao Z, et al. Strain effect in palladium nanostructures as nanozymes. *Nano Lett*. 2020;20:272–277. doi:10.1021/acs.nanolett.9b03782
21. Huang H, Wang Y, Ruditskiy A, et al. Polyol syntheses of palladium decahedra and icosahedra as pure samples by maneuvering the reaction kinetics with additives. *ACS Nano*. 2014;8:7041–7050. doi:10.1021/nn501919e
22. Liu M, Zheng Y, Zhang L, et al. Transformation of Pd nanocubes into octahedra with controlled sizes by maneuvering the rates of etching and regrowth. *J Am Chem Soc*. 2013;135:11752–11755. doi:10.1021/ja406344j
23. Li C, Sato R, Kanehara M, et al. Controllable polyol synthesis of uniform palladium icosahedra: effect of twinned structure on deformation of crystalline lattices. *Angew Chem Int Edit*. 2009;48:6883–6887. doi:10.1002/anie.200902786

24. Asmatulu E, Andalib MN, Subeshan B, et al. Impact of nanomaterials on human health: a review. *Environ Chem Lett*. 2022;20:2509–2529. doi:10.1007/s10311-022-01430-z
25. Sano S, Chan KS, DiGiovanni J. Impact of Stat3 activation upon skin biology: a dichotomy of its role between homeostasis and diseases. *J Dermatol Sci*. 2008;50:1–14. doi:10.1016/j.jdermsci.2007.05.016
26. Sano S, Itami S, Takeda K, et al. Keratinocyte-specific ablation of Stat3 exhibits impaired skin remodeling, but does not affect skin morphogenesis. *EMBO J*. 1999;18:4657–4668. doi:10.1093/emboj/18.17.4657
27. MacCarthy-Morrogh L, Martin P. The hallmarks of cancer are also the hallmarks of wound healing. *Sci Signal*. 2020;13:eaay8690. doi:10.1126/scisignal.aay8690
28. Martin P, Nunan R. Cellular and molecular mechanisms of repair in acute and chronic wound healing. *Br J Dermatol*. 2015;173:370–378. doi:10.1111/bjd.13954
29. Kobayashi T, Hashimoto K, Okumura H, et al. Endogenous EGF-family growth factors are necessary for the progression from the G1 to S phase in human keratinocytes. *J Invest Dermatol*. 1998;111:616–620. doi:10.1046/j.1523-1747.1998.00331.x
30. Reznik TE, Sang Y, Ma Y, et al. Transcription-dependent epidermal growth factor receptor activation by hepatocyte growth factor. *Mol Cancer Res*. 2008;6:139–150. doi:10.1158/1541-7786.MCR-07-0236
31. Faiola F, Liu X, Lo S, et al. Dual regulation of c-Myc by p300 via acetylation-dependent control of Myc protein turnover and coactivation of Myc-induced transcription. *Mol Cell Biol*. 2005;5:10220–10234. doi:10.1128/MCB.25.23.10220-10234.2005
32. Yang B, Chen Y, Shi J. Nanocatalytic Medicine. *Adv Mater*. 2019;31:1901778. doi:10.1002/adma.201901778
33. Paramasivam G, Kayambu N, Rabel AM, et al. Anisotropic noble metal nanoparticles: synthesis, surface functionalization and applications in biosensing, bioimaging, drug delivery and theranostics. *Acta Biomater*. 2017;49:45–65. doi:10.1016/j.actbio.2016.11.066
34. Yan J, Teo BK, Zheng N. Surface chemistry of atomically precise coinage-metal nanoclusters: from structural control to surface reactivity and catalysis. *Acc Chem Res*. 2018;51:3084–3093. doi:10.1021/acs.accounts.8b00371
35. Liu P, Qin R, Fu G, Zheng N. Surface coordination chemistry of metal nanomaterials. *J Am Chem Soc*. 2017;139:2122–2131. doi:10.1021/jacs.6b10978
36. Boomi P, Prabu HG, Mathiyarasu J. Synthesis, characterization and antibacterial activity of polyaniline/Pt-Pd nanocomposite. *Eur J Med Chem*. 2014;72:18–25. doi:10.1016/j.ejmech.2013.09.049
37. Chang Y, Cheng Y, Feng Y, et al. Upshift of the d band center toward the fermi level for promoting silver ion release, bacteria inactivation, and wound healing of alloy silver nanoparticles. *ACS Appl Mater Interfaces*. 2019;11:12224–12231. doi:10.1021/acsami.8b21768
38. Nanba D, Higashiyama S. Dual intracellular signaling by proteolytic cleavage of membrane-anchored heparin-binding EGF-like growth factor. *Cytokine Growth Factor Rev*. 2004;15:13–19. doi:10.1016/j.cytogfr.2003.10.002
39. Marikovsky M, Vogt P, Eriksson E, et al. Wound fluid-derived heparin-binding EGF-like growth factor (HB-EGF) is synergistic with insulin-like growth factor-I for Balb/MK keratinocyte proliferation. *J Invest Dermatol*. 1996;106:616–621. doi:10.1111/1523-1747.ep12345413
40. Miyata K, Yotsumoto F, Nam SO, et al. Regulatory mechanisms of the HB-EGF autocrine loop in inflammation, homeostasis, development and cancer. *Anticancer Res*. 2012;32:2347–2352.
41. Iwamoto R, Mekada E. Heparin-binding EGF-like growth factor: a juxtacrine growth factor. *Cytokine Growth Factor Rev*. 2000;11:335–344. doi:10.1016/S1359-6101(00)00013-7
42. Nakai K, Yoneda K, Moriue T, et al. HB-EGF-induced VEGF production and eNOS activation depend on both PI3 kinase and MAP kinase in HaCaT cells. *J Dermatol Sci*. 2009;55:170–178. doi:10.1016/j.jdermsci.2009.06.002
43. Inoue Y, Shimazawa M, Nakamura S, et al. Both autocrine signaling and paracrine signaling of HB-EGF enhance ocular neovascularization. *Arterioscler Thromb Vasc Biol*. 2018;38:174–185. doi:10.1161/ATVBAHA.117.310337
44. Oyagi A, Hara H. Essential roles of heparin-binding epidermal growth factor-like growth factor in the brain. *CNS Neurosci Ther*. 2012;18:803–810. doi:10.1111/j.1755-5949.2012.00371.x
45. Wierstra I. Sp1: emerging roles—Beyond constitutive activation of TATA-less housekeeping genes. *Biochem Biophys Res Commun*. 2008;372:1–13. doi:10.1016/j.bbrc.2008.03.074
46. Edwards JP, Zhang X, Mosser DM. The expression of heparin-binding epidermal growth factor-like growth factor by regulatory macrophages. *J Immunol*. 2009;182:1929–1939. doi:10.4049/jimmunol.0802703